ELEVENTH INTERNATIONAL CONFERENCE ON INTERGRANULAR AND INTERPHASE BOUNDARIES 2004

JOURNAL OF MATERIALS SCIENCE **40** (2005) 3067–3074

Effect of boundary plane on the atomic structure of [0001] $\Sigma 7$ tilt grain boundaries in ZnO

F. OBA
Department of Materials Science and Engineering, Kyoto University, Yoshida-Honmachi, Sakyo-ku, Kyoto 606-8501, Japan
E-mail: fumiyasu.oba@materials.mbox.media.kyoto-u.ac.jp

Y. SATO, T. YAMAMOTO
Department of Advanced Materials Science, The University of Tokyo, 5-1-5 Kashiwanoha, Kashiwa, Chiba 277-8651, Japan

H. OHTA, H. HOSONO
SORST, Japan Science and Technology Agency, Frontier Collaborative Research Center, Tokyo Institute of Technology, 4259 Nagatsuta, Midori-ku, Yokohama 226-8503, Japan

Y. IKUHARA
Institute of Engineering Innovation, The University of Tokyo, 2-11-16 Yayoi, Bunkyo-ku, Tokyo 113-8656, Japan

The atomic structure of [0001] $\Sigma 7$ tilt grain boundaries with $\{12\bar{3}0\}\|\{12\bar{3}0\}$, $\{14\bar{5}0\}\|\{14\bar{5}0\}$, and $\{10\bar{1}0\}\|\{35\bar{8}0\}$ boundary planes in ZnO was investigated through high-resolution transmission electron microscopy observation of fiber-textured thin films and atomistic calculations. These boundaries were found to comprise three kinds of common structural units that are characterized by fourfold- to eightfold-coordinated channels along the [0001] direction in contrast to sixfold-coordinated channels in wurtzite structure. The boundary structural units are very similar to the multiple core structures of edge dislocations with Burgers vectors of $1/3 <11\bar{2}0>$. Transformation between two of the three configurations can easily occur through an atom flipping corresponding to dislocation glide. Depending on the orientation of boundary planes with respect to the Burgers vectors, the dislocation-like units exhibit straight or zigzag arrangements with periodicities corresponding to the $\Sigma 7$ misorientation.

1. Introduction

Grain boundaries (GBs) have been a target of interest because of the significant impact on macroscopic properties. Their specific atomic and electronic structures can even generate properties that are not obtained from materials in single crystalline form. Efforts have therefore been made for the understanding of GB structures at microscopic levels. To investigate the atomic structure of GBs, high-resolution transmission electron microscopy (HRTEM) and scanning TEM (STEM) are often employed [1–5]. Their high spatial resolution can reveal not only detailed atomic structures but also local compositions and electronic structures by combining with spectroscopic techniques [4, 5]. Theoretical approaches based on empirical and first-principles methods have been effectively used for the investigation of GB atomic and electronic structures as well [6–14].

A difficulty in the investigation of GBs, however, arises from the variety and complexity in geometry and atomic structure. To overcome this, we have opted to systematically investigate GBs with relatively simple geometries. Since it requires a lot of effort to find boundaries of interest in polycrystalline specimens, the investigation of fabricated GBs, for instance, in bicrystals, is an efficient approach. A number of study on GB atomic structure in metal oxide bicrystals have been reported so far [2, 4, 5, 15–25]. In addition, bicrystals have been effectively used to investigate the relationship between the structure and the electrical property at oxide GBs [19, 26–28]. Another type of specimens suited for TEM and STEM study of GBs is fiber-textured materials in which tilt GBs with a common rotation axis are dominantly present. TEM and STEM observation is applicable to most of the GBs with an incident electron beam direction parallel to the fibers and therefore the common axis. HRTEM observations have been performed for fiber-textured ZrO_2 and GaN films to investigate tilt GBs therein [29, 30].

Recently, we have systematically investigated the atomic structure of [0001] tilt GBs in ZnO through HRTEM observation of fiber-textured ZnO films and atomistic calculations [31]. It was suggested that the GBs can be generally described by a linkage of dislocation-like structural units. Such information on

GB atomic structures in ZnO should be important to understand the GB-induced electrical properties [32–35]. In the present study the atomic structure of high coincidence GBs with a $\Sigma 7$ misorientation [36] was investigated in detail by HRTEM and atomistic calculations. These GBs have periodic structures with the smallest or relatively small periodicities among the [0001] tilt boundaries, which are suited for a detailed analysis. $\Sigma 7$ boundaries with three kinds of boundary planes, $\{12\bar{3}0\}\|\{12\bar{3}0\}$, $\{14\bar{5}0\}\|\{14\bar{5}0\}$, and $\{10\bar{1}0\}\|\{35\bar{8}0\}$, were examined to elucidate the relationship between the atomic structures and boundary planes.

2. Experimental and computational procedures

ZnO thin films with a [0001] fiber-texture were fabricated on quartz-glass substrates by the pulsed-laser deposition. The detail of deposition conditions can be found elsewhere [31]. The films were subjected to post-annealing at 800°C for 3 h in air to obtain energetically favorable GBs. In order to observe [0001] tilt GBs from the direction parallel to the [0001], plan-view TEM foils were prepared by back-thinning the annealed specimens from the substrate side. This procedure includes mechanical grinding and dimpling down to about 20 μm and argon-ion-beam thinning to an electron transparency using DuoMill Model 600 (Gatan, Inc., Pleasanton, CA) with gun energies of 3–4 keV and a beam angle of 13°. The TEM observation was conducted on a JEM-4010 operated at 400kV (JEOL, Tokyo, Japan).

Atomistic calculations were conducted for $\{12\bar{3}0\}\|\{12\bar{3}0\}$ and $\{14\bar{5}0\}\|\{14\bar{5}0\}\Sigma 7$ GBs using the GULP program code [37] based on the lattice statics method. Under three-dimensional periodic boundary conditions, the total lattice energy, described as a long-range Madelung potential and short-range Buckingham potentials, was iteratively minimized to achieve the optimum atomic positions in simulation cells at 0 K. A potential parameter set reported by Lewis and Catlow [38] was employed, which has been confirmed to reproduce lattice and elastic constants of ZnO fairly well [12], and to give boundary atomic configurations very close to those obtained by first-principles calculations [13]. Supercells containing two identical $\Sigma 7$ boundaries were constructed to match the three-dimensional periodic boundary conditions. We have previously modeled the atomic configurations of the $\{12\bar{3}0\}\|\{12\bar{3}0\}$ boundary using this method [31]. Two kinds of supercells composed of about 180 and 290 atoms where the distances between the boundaries are 2.5 and 4 nm, respectively, were used to examine the convergence of the energy with respect to the cell size. The energy differences were confirmed to be less than 0.01 Jm^{-2} for equilibrium boundary configurations shown later in Fig. 3. Based on these results, supercells containing about 220 atoms with a boundary-boundary distance of 1.8 nm were chosen for the calculations of the $\{14\bar{5}0\}\|\{14\bar{5}0\}$ GB in this study. The geometry optimization, namely energy minimization, was performed for the GB supercells in various three-dimensional translation states. Increments of about 0.015 nm and 0.01 nm were used for the directions parallel and perpendicular to the GB, respectively. The boundary energy was evaluated as a function of the translation states, and configurations in the local energy minima were selected as equilibrium structures.

Using atomic configurations modeled by the atomistic calculations, HRTEM image simulations were carried out using the MacTempas program (Total Resolution, Berkeley, CA) based on the multi-slice method [39]. HRTEM images were calculated as a function of defocus and specimen thickness to search conditions that give the best agreement with experimental images.

3. Results and discussion

Fig. 1a shows a HRTEM image of a [0001] tilt GB observed with an incident electron beam direction parallel to the [0001] direction of both grains. The rotation angle was estimated at $20.1 \pm 0.2°$ from Fourier transforms of the HRTEM image, which is close to that of the $\Sigma 7$ misorientation, 21.79°. The boundary is curving and therefore shows various characters in atomic structure. In Fig. 1b and c, parts of the boundary are highlighted. A nearly symmetric structure is recognized at the area shown in Fig. 1b. $\{10\bar{1}0\}$ planes in the upper and lower grains making an angle of 39.9° are indicated by lines to clarify the symmetric feature, but the lowest rotation angle are given by the $\{11\bar{2}0\}$ planes as $60-39.9 = 20.1°$. The boundary plane approximately corresponds to one of the $\{12\bar{3}0\}$ for both grains, which provide a symmetric structure under the $\Sigma 7$ misorientation.

The portion of the GB presented in Fig. 1c is somewhat different in geometry and atomic structure from that shown in Fig. 1b. In the image area, the GB is making a turn around the middle. In the left-half, the boundary is located almost on a $(10\bar{1}0)$ plane of the upper grain to give an asymmetric structure. Moving on to the right-hand side, the boundary is shifted toward the lower grain to form a nearly symmetric structure. These structures approximately correspond to the $\{10\bar{1}0\}\|\{35\bar{8}0\}$ and the $\{14\bar{5}0\}\|\{14\bar{5}0\}$, respectively. The latter is the other set of the planes that gives a symmetric structure under the $\Sigma 7$ misorientation. Basically, the local atomic structure of GBs should depend on the local boundary plane. However, these GBs with $\{12\bar{3}0\}\|\{12\bar{3}0\}$, $\{14\bar{5}0\}\|\{14\bar{5}0\}$, and $\{10\bar{1}0\}\|\{35\bar{8}0\}$ boundary planes seem to have common structural units as will be discussed in detail below. In addition, there are some similarities between the GB structural units and edge dislocation core structures. The image area shown in Fig. 1a includes an edge dislocation, which is highlighted in Fig. 1d. The Burgers circuit, which was made on the basis of bright spots representing the primitive cell edges along the [0001] direction (detailed later), indicate that the dislocation has an edge component with an Burgers vector $\mathbf{b} = 1/3\langle 11\bar{2}0\rangle$. The local atomic structure of such isolated edge dislocations will also be discussed in comparison with the GB structures.

Fig. 2a shows a HRTEM image of a $\{12\bar{3}0\}\|\{12\bar{3}0\}$ symmetric structure found at a GB with an estimated

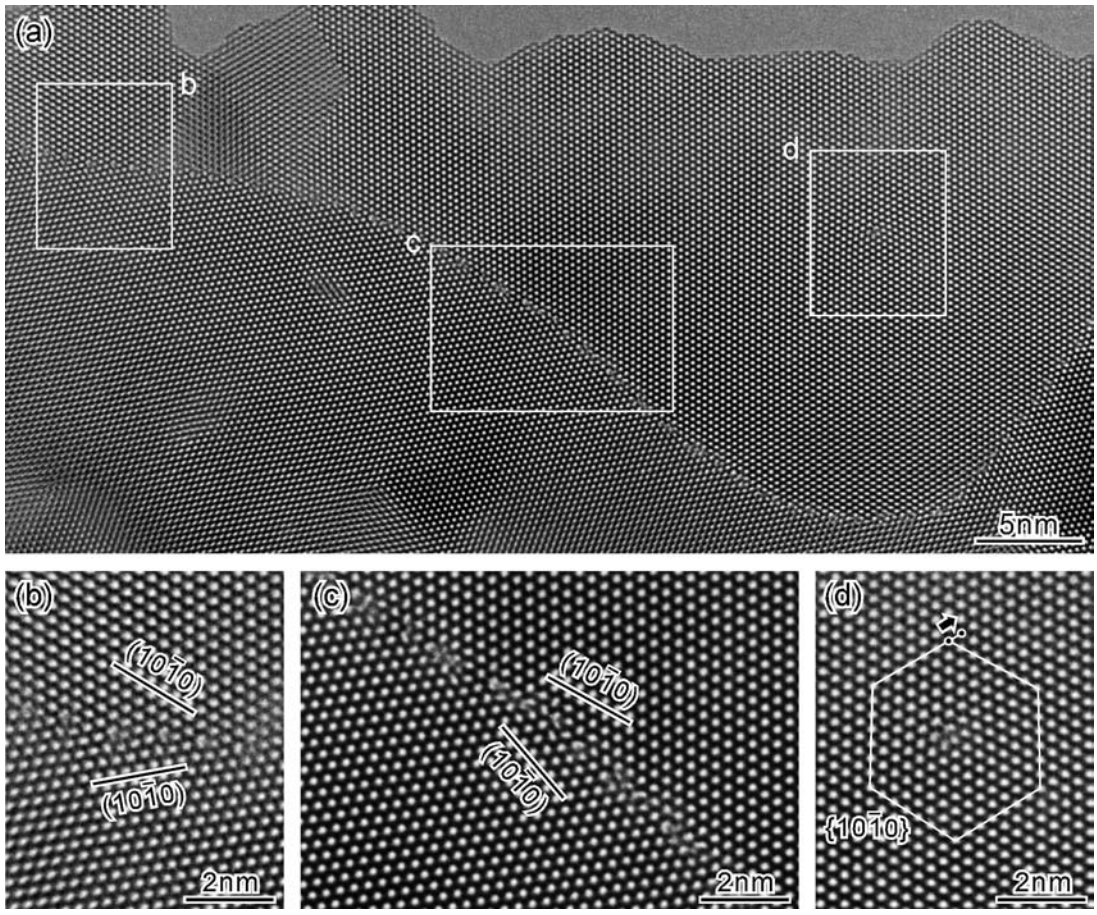

Figure 1 (a) HRTEM image of a [0001] tilt GB with a misorientation close to Σ7. The incident electron beam direction is parallel to the [0001] direction in both grains. (b–d) Enlargements of areas labeled correspondingly in Fig. (a). (b) Near $\{12\bar{3}0\}\|\{12\bar{3}0\}$ symmetric structure. (c) Near $\{10\bar{1}0\}\|\{35\bar{8}0\}$ asymmetric and $\{14\bar{5}0\}\|\{14\bar{5}0\}$ symmetric structures. (d) Edge dislocation. A Burgers circuit is drawn along $\{10\bar{1}0\}$ planes. The arrow denotes the resultant Burgers vector of $1/3\ <11\bar{2}0>$.

rotation angle of $20.0 \pm 0.2^{\circ}$. Systematic image simulations indicated that under the imaging condition employed, the bright spots approximately correspond to the open channels along the [0001] direction in ZnO with wurtzite structure. The distance between the open channels and therefore bright spots in the HRTEM images is equal to the lattice constant a, 0.325 nm [40]. The open channels have the highest symmetry as well as the atomic columns, and represent the edges of the primitive cell. In Fig. 2, the GB structural units are indicated by quadrilaterals drawn along the bright spots. It is recognized that the two units from the left, which are denoted by dotted quadrilaterals, have image features somewhat different from the others indicated by solid lines. The difference can be summarized as: (i) the dotted units are narrower in the direction perpendicular to the GB; (ii) the spots located inside the dotted units are weaker in contrast; (iii) the spots at the right-hand edges of the units have a circular shape, while those at the solid units are U-shaped; and (iv) the spots at the upper and lower edges are elongated in the dotted units. These differences indicate that there are at least two kinds of units for the Σ7 GB.

Fig. 2b and c shows two HRTEM images of isolated dislocations. The edge components of the Burgers vectors were determined to be $1/3<11\bar{2}0>$ for both dislocations, as in the case of the dislocation shown in Fig. 1d. A screw component may be absent since no anisotropic contrast was observed with an incident beam tilted. Interestingly, the core structures described by quadrilaterals show similarity to the structural units of the Σ7 GB. In addition, differences found between the two kinds of the GB units can be recognized between the two dislocations. The one shown in Fig. 2b is similar in image feature to the solid units in Fig. 2a while the other shown in Fig. 2c looks like the dotted units. The dislocations seem to have multiple configurations as well.

The atomistic calculations for the $\{12\bar{3}0\}\|\{12\bar{3}0\}$ GB also suggested the presence of multiple structural units. Some types of equilibrium configurations were obtained with nearly the same boundary energies [12, 31]. Among them, three configurations and their simulated images that showed good agreements with experimental images of the Σ7 GBs are presented in Fig. 3. The configuration given in Fig. 3a contains a relatively large open space at the GB core. It is composed of a linkage of channels surrounded by five and seven atomic columns, respectively. The structural unit of the configuration shown in Fig. 3b has U-shaped channels surrounded by eight atomic columns at the right-hand side edge. The channel located inside the unit is sixfold coordinated as in the case of the perfect crystal. The unit shown in the Fig. 3c has fourfold and sixfold coordinated channels.

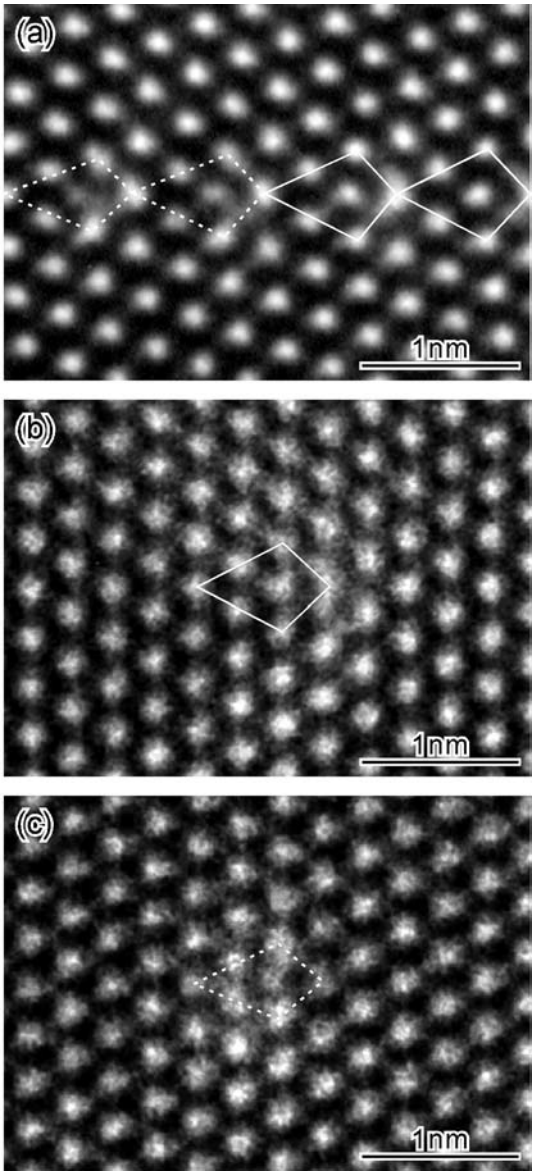

Figure 2 (a) HRTEM image of a near $\{12\bar{3}0\}\|\{12\bar{3}0\}\Sigma 7$ boundary. The structural units are denoted by solid and dotted quadrilaterals. (b), (c) Typical HRTEM images of isolated edge dislocations with Burgers vectors of $1/3<11\bar{2}0>$.

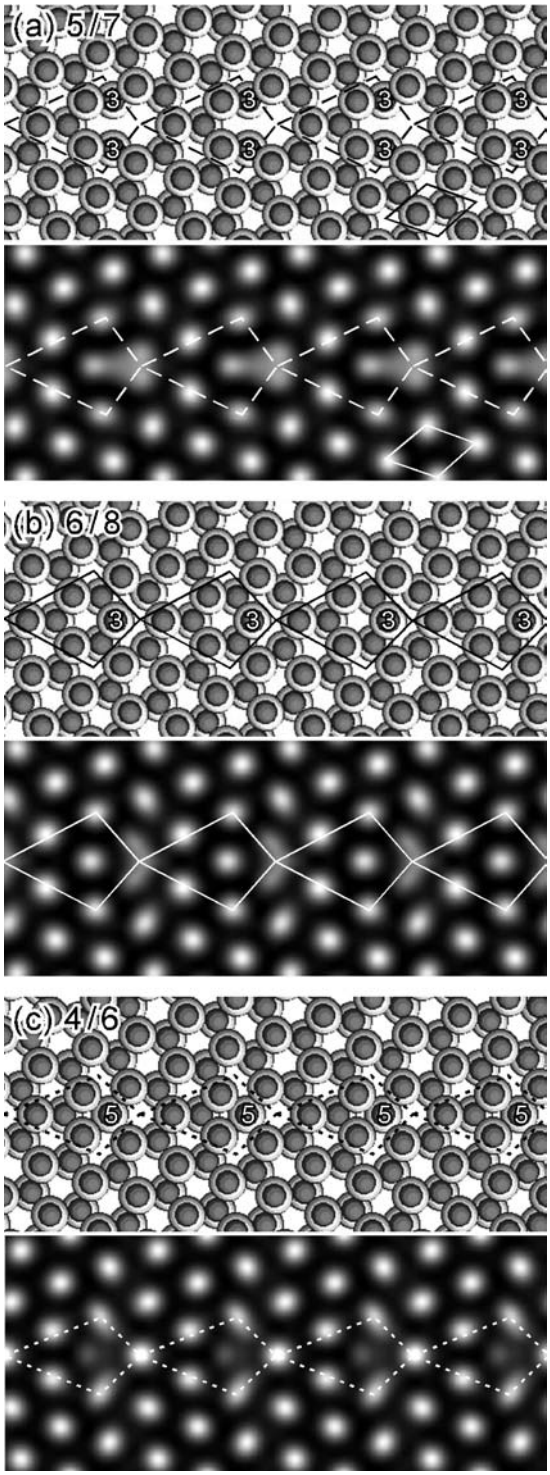

Figure 3 Modeled atomic configurations of the $\{12\bar{3}0\}\|\{12\bar{3}0\}$ $\Sigma 7$ GB viewed from the $[000\bar{1}]$ direction (upper) and their simulated HRTEM images (lower). The smaller and larger circles designate Zn and O atoms, respectively. Columns containing miscoordinated atoms are labeled with coordination numbers. The small and larger quadrilaterals indicate the primitive cell and GB structural units, respectively. The configurations shown in the panels (a), (b), and (c) are noted as 5/7, 6/8, and 4/6 on the basis of the coordination numbers of open channels, respectively.

Based on these shapes of the open channels, the configurations will be noted 5/7, 6/8, and 4/6 hereafter, as indicated in the figure. Relating to the presence of the open channels that have different coordination numbers from six, some atoms are coordinated by three or five first-nearest neighbors in contrast to the fourfold coordination in wurtzite structure. The columns containing these atoms are labeled with the coordination numbers in the figure. The 5/7, 6/8, and 4/6 configurations showed boundary energies of 1.69, 1.54, and 1.54 Jm^{-2}, respectively. The higher energy of the 5/7 configuration than the others can be partly attributed to the presence of twice number of the miscoordinated atoms per structural units.

Simulated HRTEM images shown in the lower panels of the figures were obtained with a foil thickness of 5 nm and a defocus of -26 nm, which gave the best agreement with the experimental image shown in Fig. 2a. A comparison between the modeled atomic configurations and the simulated images indicates that atomic columns located parallel to the [0001] direction appear dark and the bright spots approximately represent open channels as mentioned above. The shapes of the channels specific to the GB configurations are reflected as bright spots in the simulated images as well. Based on the results of the atomistic calculations and

image simulations, the solid and dotted structural units of the Σ7 GB and edge dislocations shown in Fig. 2 can be assigned to the 6/8 and 4/6 configurations, respectively. These configurations were frequently observed at Σ7 GBs and edge dislocations [31]. Units that show image features between the 5/7 and 6/8 configurations were also found. Therefore, the 5/7 configurations may coexist although it was difficult to surely differentiate them from the 6/8 configuration. In GaN that also has wurtzite structure, the three configurations, namely 5/7, 6/8, and 4/6, have been modeled for [0001] tilt GBs and edge dislocations with Burgers vectors of $\mathbf{b} = 1/3 <11\bar{2}0>$. [41–45] Among them, the 6/8 and 5/7 configurations have been experimentally observed at a Σ7 GB and dislocations in GaN [30, 46].

It has been pointed out that the structural transition can readily take place between the 6/8 and 4/6 configurations by the glide of dislocations in GaN, and these two configurations can be connected with the 5/7 configuration by dislocation climb [44]. The occurrence of such a structural transition was also implied for Σ7 GB in the present study. Fig. 4a and b shows HRTEM images of a Σ7 GB taken from nearly the same area with an interval of about 10 sec. Interestingly, the structures and positions of GBs are different between the two images. In the former, all the units can be assigned to the 6/8 or 5/7 configurations; some of them have image characters between the two configurations and the further assignment is difficult to make. Turning to the latter, some units represented by dotted quadrilaterals show image features particular to the 4/6 configuration, suggesting

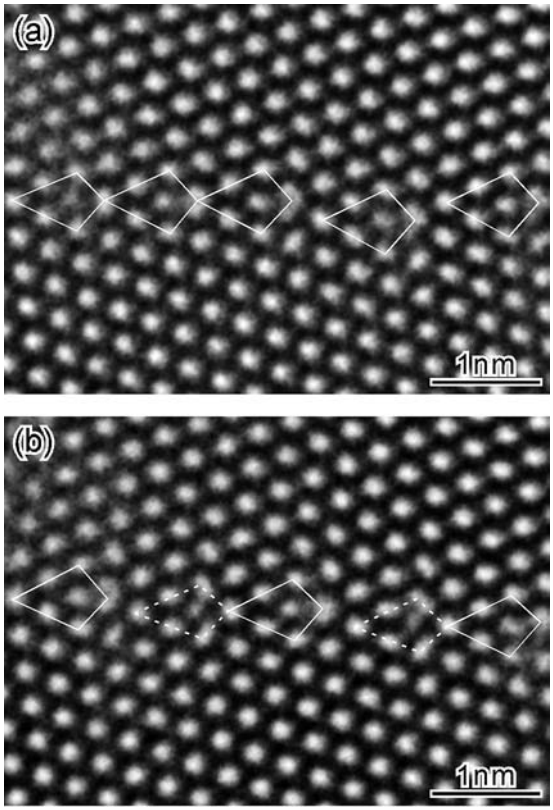

Figure 4 HRTEM images of a near $\{12\bar{3}0\}\|\{12\bar{3}0\}$ GB taken successively from almost the same image area with an interval of about 10 s. The 5/7 and 6/8 type structural units are denoted by solid quadrilaterals, while the 4/6 units are dotted.

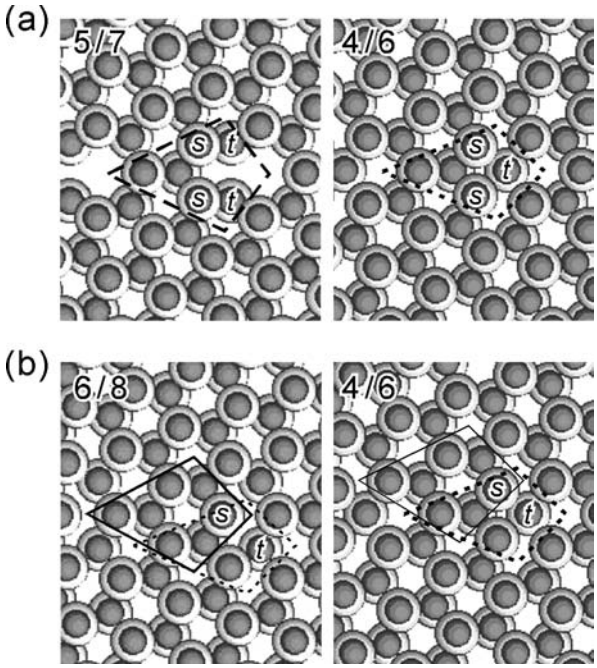

Figure 5 Atomic structure models showing the relationship between (a) the 5/7 and 4/6 configurations and (b) the 6/8 and 4/6 configurations. The smaller and larger circles designate Zn and O atoms, respectively. Differences between the structural units can be represented by the location and number of atomic columns labeled *s* and *t*.

that structural transition has occurred. In Figs 5a and b, the relationship between the 5/7 and 4/6 configurations and the 6/8 and 4/6 configurations is illustrated using the atomic configuration models, respectively. The 4/6 configuration can be made from the 5/7 configuration by removing and sharing one of the atomic columns labeled *t*, as shown in Fig. 5a. On the other hand, the transition from the 6/8 configuration to the 4/6 configuration does not require the change in the number of atoms. The atomic column labeled *s* is little separated from the one labeled *t* in the 6/8 configuration as shown in the left panel of Fig. 5b. If these atomic columns become closer and bonded, it results in the formation of the 4/6 configuration. This atom flipping can correspond to a dislocation glide as has been suggested for GaN [44]. The structural transition is therefore accompanied by the shift of the structural units toward one of the $<11\bar{2}0>$ directions. Such a mechanism may have taken place at the GB shown in Fig. 4a and b.

The dislocation-like structural units were also recognized at Σ7 GBs with different boundary planes. Fig. 6 displays a HRTEM image of a 20.1° GB with near $\Sigma7\{14\bar{5}0\}\|\{14\bar{5}0\}$ misorientation along with a modeled atomic configuration and its simulated HRTEM image. As in the case of the $\{12\bar{3}0\}\|\{12\bar{3}0\}$ GB, a configuration that showed a good agreement with the experimental image was selected from a number of equilibrium configurations obtained by the atomistic calculations. The calculated GB energy of 1.86 Jm^{-2} is one of the smallest among them. The condition of the image simulation was chosen to be a foil thickness of 4 nm and a defocus of −36 nm. The comparison between the experimental and simulated images indicates that this GB can be described by the dislocation-like structural

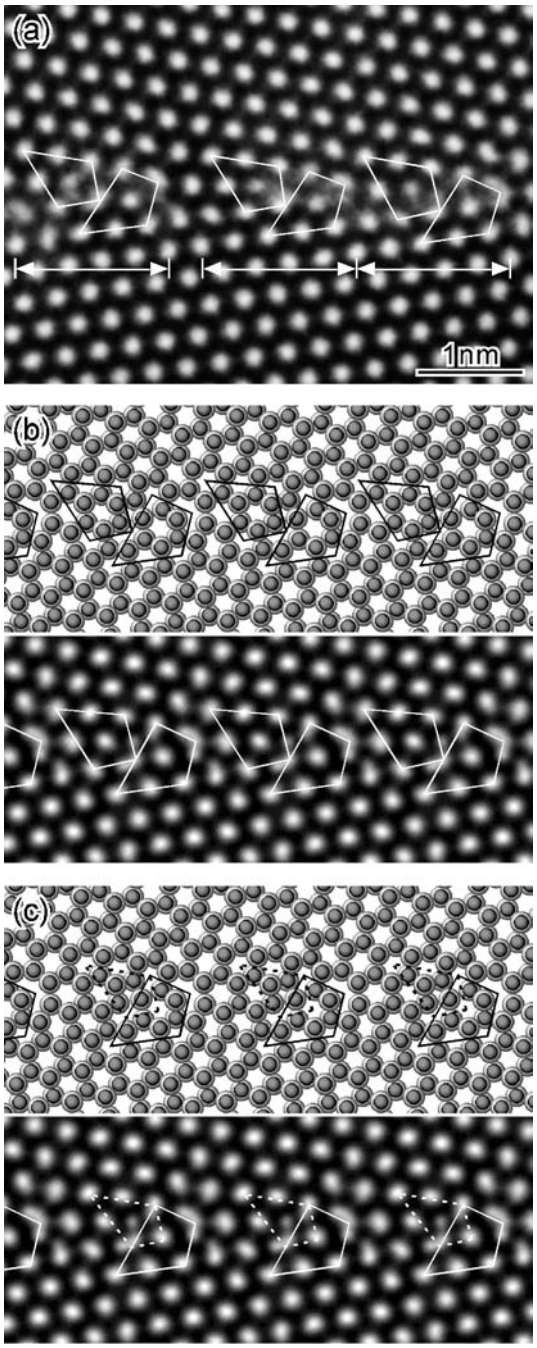

Figure 6 (a) HRTEM image of a $\{14\bar{5}0\}\|\{14\bar{5}0\}\Sigma7$ GB. The arrows and quadrilaterals indicate periodicity and dislocation-like structural units, respectively. (b) GB configuration modeled by atomistic calculation (upper) and its simulated HRTEM image (lower). The smaller and larger circles denote Zn and O atoms, respectively. (c) The same configuration and simulated image as that shown in Fig. (b) but dislocation-like units are described differently.

units as well as the $\{12\bar{3}0\}\|\{12\bar{3}0\}$ GB. The arrangement of the units, however, is zigzag rather than straight in this case. This can be understood by the orientation of the boundary plane. If the boundary normal is close to the direction of the Burgers vector of the edge dislocations, $1/3 <11\bar{2}0>$, i.e., the boundary plane is near one of the $\{11\bar{2}0\}$ planes, the misorientation can be readily accommodated by the dislocations as in the case of so-called low angle boundaries. On the other hand, when the boundary plane is relatively close to one of the $\{10\bar{1}0\}$ planes that is parallel to the Burgers vector, a zigzag arrangement is required to accommodate the misorientation by dislocations with $\mathbf{b} = 1/3 <11\bar{2}0>$. Such a tendency has been generally found at [0001] tilt GBs in our previous study [31]. For the $\Sigma7$ GB, the $\{12\bar{3}0\}\|\{12\bar{3}0\}$ and $\{14\bar{5}0\}\|\{14\bar{5}0\}$ GBs should be categorized into the former and the latter cases, respectively. At the $\{14\bar{5}0\}\|\{14\bar{5}0\}$ GB, a pair of the dislocation-like structural units oriented toward different directions can be considered as a periodicity unit. There are spaces between the pairs of the dislocation-like units so that the geometry is consistent with the $\Sigma7$. In the modeled configuration, an average distance between dislocation cores is 0.75 nm, which is somewhat smaller than that of the 6/8 and 4/6 configurations of the $\{12\bar{3}0\}\|\{12\bar{3}0\}$ GB, 0.86 nm^{-2}. This can be a part of the reason for the higher boundary energy, 1.86 v.s. 1.54 Jm^{-2}, although the difference in the arrangement of the dislocation-like units and the local atomic relaxation should also have affected the energies.

In the experimental image shown in Fig. 6a, the periodicity is not perfect; a larger space can be recognized between the first and second pairs of the structural units from the left. This is probably due to the deviation in rotation angle by 1.7° from the exact one. Such shift of structural units can also be interpreted on the basis of the displacement shift complete [30, 47]. Concerning the local atomic structure of the dislocation-like units, most of them look similar to the 6/8 or 5/7 configuration. The exact assessment, however, is difficult to make since the units are somewhat distorted from the original symmetric structure particularly at this GB with a zigzag arrangement. This is also the case with the modeled structure. In Figs 6b and c, the same atomic configurations are depicted with dislocation-like units described differently. The periodicity unit can be represented by a pair of the 6/8 units (Fig. 6b), or it can be considered as a combination of the 6/8 and 4/6 units (Fig. 6c). In detail, some structural units in Fig.6a have image features between the 6/8 and 4/6 units.

In Fig. 7, a HRTEM image of 20.1° GB near $\Sigma7$ $\{10\bar{1}0\}\|\{35\bar{8}0\}$ is presented. This is an enlargement of part of the GB depicted in Fig. 1a and shows nearly the same position as that highlighted in Fig. 1c although the image has been rotated. In most of the image area around the middle, the boundary plane is located near one of the $\{10\bar{1}0\}$ planes of the lower grain to form an asymmetric structure. This GB is composed of dislocation-like units with two types of the Burgers vector directions as in the case of the $\{14\bar{5}0\}\|\{14\bar{5}0\}$ GB. Many of units look similar to the 6/8 configuration although distortion makes the detailed assignment difficult. The arrangement of the units is not regular presumably due to the imperfectness in the misorientation.

Moving to the left-hand side, the boundary plane is shifted toward the upper grain to form a structure near the $\{14\bar{5}0\}\|\{14\bar{5}0\}$. An alternate arrangement of two kinds of the dislocation units can be recognized as in the case of the GB shown in Fig. 6a, but the separations between the units are larger. Actually, this image was taken from almost the same area as that in Fig. 6a about 10 sec before. The structural units may easily move as

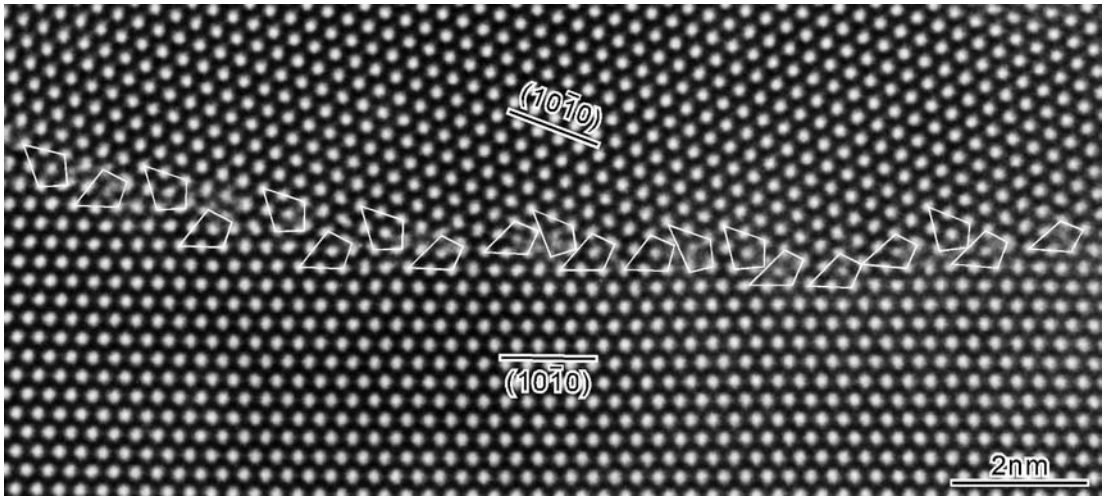

Figure 7 HRTEM image of a Σ7 boundary. Structural units are denoted by solid quadrilaterals. The boundary plane varies from left to right in the order of {14$\bar{5}$0}‖{14$\bar{5}$0}, {10$\bar{1}$0}‖{35$\bar{8}$0}, and {12$\bar{3}$0}‖{12$\bar{3}$0}.

in the case of the {12$\bar{3}$0}‖{12$\bar{3}$0} GB shown in Fig. 4. Turning to the right-hand side, the structure becomes closer to the {12$\bar{3}$0}‖{12$\bar{3}$0}. The ratio of the units orientated parallel to the GB plane is increased although there still is a unit that is oriented differently from the others because of the incompleteness in the structural transition. The {12$\bar{3}$0}‖{12$\bar{3}$0}, {14$\bar{5}$0}‖{14$\bar{5}$0}, and {10$\bar{1}$0}‖{35$\bar{8}$0} structures can thus be connected with one another by the change in the arrangement and orientation of the common structural units.

4. Conclusions

HRTEM observation was conducted for [0001] tilt Σ7 {12$\bar{3}$0}‖{12$\bar{3}$0}, {14$\bar{5}$0}‖{14$\bar{5}$0}, and {10$\bar{1}$0}‖{35$\bar{8}$0} GBs in fiber-textured ZnO thin films to investigate the relationship between their atomic structures and boundary planes. The atomistic calculations combined with HRTEM image simulations indicated that three kinds of structural units can coexist at the Σ7 GBs. These are characterized by fourfold- to eightfold-coordinated channels located along the [0001] direction. The atomic structures of the units are very similar to those of edge dislocations with Burgers vectors of 1/3 <11$\bar{2}$0>. A structural transformation between two of the three configurations can easily take place through an atom flipping corresponding to dislocation glide. The structural units are common to the three kinds of GBs but arranged differently depending on the orientation of boundary planes with respect to the Burgers vectors.

Acknowledgments

We thank Dr. J. D. Gale for allowing us to use the GULP program code. This study was supported by a Grant-in-Aid for Scientific Research from the Ministry of Education, Culture, Sports, Science and Technology of Japan, and the Japan Society for the Promotion of Science.

References

1. O. L. KRIVANEK, S. ISODA and K. KOBAYASHI, *Philos. Mag.* **36** (1977) 931.
2. K. L. MERKLE and D. J. SMITH, *Phys. Rev. Lett.* **59** (1987) 2887.
3. F. ERNST, M. W. FINNIS, D. HOFMANN, T. MUSCHIK, U. SCHÖNBERGER, U. WOLF and M. METHFESSEL, *ibid.* **69** (1992) 620.
4. M. M. MCGIBBON, N. D. BROWNING. M. F. CHISHOLM, A. J. MCGIBBON, S. J. PENNYCOOK, V. RAVIKUMAR and V. P. DRAVID, *Science* **266** (1994) 102.
5. N. D. BROWNING, J. P. BUBAN, H. O. MOLTAJI, S. J. PENNYCOOK, G. DUSCHER, K. D. JOHNSON, R. P. RODRIGUES and V. P. DRAVID, *Appl. Phys. Lett.* **74** (1999) 2638.
6. D. M. DUFFY and P. W. TASKER, *Phil. Mag. A* **47** (1983) 817.
7. D. WOLF, *J. Am. Ceram. Soc.* **67** (1984) 1.
8. M. KOHYAMA, *Modelling Simul. Mater. Sci. Eng.* **10** (2002) R31.
9. I. DAWSON, P. D. BRISTOWE, M. H. LEE, M. C. PAYNE, M. D. SEGALL and J. A. WHITE, *Phys. Rev. B* **54** (1996) 13727.
10. S. D. MO, W. Y. CHING, M. F. CHISHOLM and G. DUSCHER, *ibid.* **60** 2416 (1999).
11. S. FABRIS and C. ELSÄSSER, *ibid.* **64** (2001) 245117.
12. F. OBA, I. TANAKA, S. R. NISHITANI, H. ADACHI, B. SLATER and D. H. GAY, *Phil. Mag. A* **80** (2000) 1567.
13. F. OBA, S. R. NISHITANI, H. ADACHI, I. TANAKA, M. KOHYAMA and S. TANAKA, *Phys. Rev. B* **63** (2001) 045410.
14. J. M. CARLSSON, B. HELLSING, H. S. DOMINGOS and P. D. BRISTOWE, *J. Phys.: Condens. Matter* **13** (2001) 9937.
15. T. HÖCHE, P. R. KENWAY, H.-J. KLEEBE, M. RÜHLE and P. A. MORRIS, *J. Amer. Ceram. Soc.* **77** (1994) 339.
16. U. DAHMEN, S. PACIORNIK, I. G. SOLORZANO and J. B. VANDERSANDE, *Inter. Sci.* **2** (1994) 125.
17. N. KISELEV, F. SARRAZIT, E. A. STEPANTSOV, E. OLSSON, T. CLAESON, V. I. BONDARENKO, R. C. POND and N. A. KISELEV, *Phil. Mag. A* **76** (1997) 633.
18. Y. IKUHARA, T. WATANABE, T. SAITO, H. YOSHIDA and T. SAKUMA, *Mater. Sci. Forum* **284-286** (1999) 273.
19. T. YAMAMOTO, K. HAYASHI, Y. IKUHARA and T. SAKUMA, *J. Amer. Ceram. Soc.* **83** (2000) 1527.
20. E. C. DICKEY, X. D. FAN and S. J. PENNYCOOK, *ibid.* **84** (2001) 1361.
21. S. NUFER, A. G. MARINOPOULOS, T. GEMMING, C. ELSÄSSER, W. KURTZ, S. KÖSTLMEIER and M. RÜHLE, *Phys. Rev. Lett.* **86** (2001) 5066.
22. N. SHIBATA, F. OBA, T. YAMAMOTO, Y. IKUHARA and T. SAKUMA, *Philos. Mag. Lett.* **82** (2002) 393.

23. Z. ZHANG, W. SIGLE and M. RÜHLE, *Phys. Rev. B* **66** (2002) 094108.
24. H. NISHIMURA, K. MATSUNAGA, T. SAITO T, T. YAMAMOTO and Y. IKUHARA, *J. Amer. Ceram. Soc.* **86** (2003) 574.
25. N. SHIBATA, F. OBA, T. YAMAMOTO and Y. IKUHARA, *Philos. Mag.* **84** (2004) 2381.
26. Y. SATO, F. OBA, T. YAMAMOTO, Y. IKUHARA and T. SAKUMA, *J. Amer. Ceram. Soc.* **85** (2002) 2142.
27. F. OBA, Y. SATO, T. YAMAMOTO, Y. IKUHARA and T. SAKUMA, *ibid.* **86** (2003) 1616.
28. Y. SATO, F. OBA, M. YODOGAWA, T. YAMAMOTO and Y. IKUHARA, *J. Appl. Phys.* **95** (2004) 1258.
29. K. L. MERKLE, G.-R. BAI, Z. LI, C.-Y. SONG and L. J. THOMPSON, *Phys. Stat. Sol.* (a) **166** 73 (1998).
30. V. POTIN, P. RUTERANA, G. NOUET, R. C. POND and H. MORKOÇ, *Phys. Rev. B* **61** (2000) 5587.
31. F. OBA, H. OHTA, Y. SATO, H. HOSONO, T. YAMAMOTO and Y. IKUHARA, *ibid.* **70** (2004) 125415.
32. D. R. CLARKE, *J. Amer. Ceram. Soc.* **82** (1999) 485.
33. M. MATSUOKA, *Jpn. J. Appl. Phys.* **10** (1971) 736.
34. K. MUKAE, K. TSUDA and I. NAGASAWA, *ibid.* **16** (1977) 1361.
35. G. E. PIKE and C. H. SEAGER, *J. Appl. Phys.* **50** (1979) 3414.
36. D. G. BRANDON, B. RALPH, S. RANGANATHAN and M. S. WALD, *Acta. Metall.* **12** (1964) 813.
37. J. D. GALE, *J. Chem. Soc. Faraday Trans.* **93** (1997) 629.
38. G. V. LEWIS and C. R. A. CATLOW, *J. Phys. C: Solid State Phys.* **18** (1985) 1149.
39. J. M. COWLEY and A. F. MOODIE, *Acta Cryst.* **10** (1957) 609.
40. S. C. ABRAHAMS and J. L. BERNSTEIN, *Acta. Crystallogr. Sect.* B **25** (1969) 1233.
41. J. ELSNER, R. JONES, P. K. SITCH, V. D. POREZAG, M. ELSTNER, TH. FRAUENHEIM, M. I. HEGGIE, S. ÖBERG and P. R. BRIDDON, *Phys. Rev. Lett.* **79** (1997) 3672.
42. J. CHEN, P. RUTERANA and G. NOUET, *Mater. Sci. Eng.* **B82** (2001) 117.
43. A. BÉRÉ and A. SERRA, *Phys. Rev. B* **66** (2002) 085330.
44. *Idem.*, *ibid.* **65** (2002) 205323.
45. J. CHEN, P. RUTERANA and G. NOUET, *Phys. Rev. B* **67** (2003) 205210.
46. Y. XIN, S. J. PENNYCOOK, N. D. BROWNING, P. D. NELLIST, S. SIVANANTHAN, F. OMNÉS, B. BEAUMONT, J. P. FAURIE and P. GIBART, *Appl. Phys. Lett.* **72** (1998) 2680.
47. W. BOLLMANN, "Crystal Defects and Crystalline Interfaces" (Springer-Verlag, Berlin, 1970).

Received 8 September 2004
and accepted 31 January 2005